Vietnam Journal of Catalysis and Adsorption
Tạp chí xúc tác và hấp phụ Việt Nam

https://chemeng.hust.edu.vn/jca/

Degradation of recalcitrant organic pollutants by modified TiO_2 photocatalysts

Nguyen Thi Lan

Faculty of Natural Sciences, Quy Nhon University, 170 An Duong Vuong, Quy Nhon, Binh Dinh
Email: nguyenthilan@qnu.edu.vn

ARTICLE INFO

Received: 20/02/2022
Accepted: 20/4/2022
Published: 15/6/2022

Keywords:

Photocatalyst TiO_2, a doped, tetracycline antibiotics, ilmenite.

ABSTRACT

Non-metallic C, N, and S doped TiO_2 materials were prepared using the hydrothermal method from titanyl sulfate solution with different doped precursors. The influence of non-metallic elements on crystal structure, morphology, surface area, bonding state, and light absorption ability of materials was studied through XRD, SEM, BET spectra, and UVis - DRS. The formation of new Ti-O-C, O-N-Ti bonds, the insertion of non-metallic elements into the TiO_2 crystal lattice, or the replacement of Ti^{4+} with S^{6+} has created a redshift in the bandgap energy of the material doping. The increase in the specific surface area of the doped materials is their enhanced photocatalytic activity. The results demonstrate that the C, N, and S co-doped TiO_2 (TH-TiO_2) material has the best action for degrading tetracycline (TC) antibiotics.

Introduction

Tetracycline (denoted as TC) is one of the most widely used antibiotics in veterinary medicine and aquaculture [1]. Due to its poor absorption, most of them are not metabolized and excreted in the feces and urine as the original compounds. Tetracycline is usually detected at 0.07-1.34 µg/L in surface water samples. The most dangerous effect of antibiotics in the environment is to create favorable conditions for developing resistant strains of bacteria and cause the current phenomenon of antibiotic resistance [2]. Therefore, the elimination of tetracycline should be of considerable concern. Most of the tetracycline detected in surface water, drinking water, and mud is due to the ineffective elimination of traditional and biological methods. New treatment methods need to be developed to reduce the amount of tetracycline released into the environment. Advanced oxidation processes (AOPs) such as photochemical processes [1], [3], ozonation [4], ultrasonic waves [5], and Fenton processes [6] are considered effective technologies to decompose antibiotics pollutants in aqueous solution. Among the AOPs, the photocatalytic process based on titanium dioxide is one of the most promising technologies. TiO_2, with the preeminent properties such as high photocatalytic activity, super wetting, is very durable, non-toxic, increased reserves, etc., has been studied and applied widely [7]. However, with a bandgap of about 3.2 - 3.5 eV, TiO_2 material can only give a catalytic effect in the ultraviolet (UV) light region. The portion of UV radiation in the solar spectrum to the earth's surface is only about 5%, so the use of this source of radiation for TiO_2 photocatalytic treatment is limited. To expand the use of solar radiation energy in the visible light area into the photocatalytic reaction, it is necessary to reduce the bandgap energy of TiO_2 or shift the light absorption of TiO_2 from the UV to the

https://doi.org/10.51316/jca.2022.035

visible region. Many studies have suggested that TiO_2 doped with nonmetal elements such as C, F, N, and S can extend the absorption spectrum to the visible light region [8].

Atanelov et al. [9] theoretically studied TiO_2 doped with C and N atoms at two different concentrations. They found that dopants decrease the bandgap, enhancing the TiO_2 photocatalytic activity. States created by the doping process must localize close to the valence band maximum (VBM) or the conduction band minimum (CBM) since conditions spread along the bandgap may act as a recombination center [9]. Sakthivel and Kisch [10] found that C-doping TiO_2 is five times more efficient than N-doping in the degradation of 4-chlorophenol when artificial light (≥ 455 nm) is used. Tian and Liu [11] showed that high S concentrations as a TiO_2 dopant induced a light absorption redshift [12].

TiO2 was prepared from ilmenite ore using the sulphuric acid method in the present study. Then doping of C, N, and S elements into TiO2 was performed through the hydrothermal process of TiO2 thiourea. Photocatalytic decomposition reaction in the visible region of tetracycline on C-TiO_2, N-TiO_2, S-TiO_2, and C-N-S tridoped TiO_2 composite were investigated.

Experimental

Materials and synthesis

Ilmenite ore was provided kindly by Binh Dinh company (Vietnam). The chemical composition analyzed Atomic Absorption Spectroscopy (AAS) are TiO_2 (49.54%), FeO (32.69%), Fe_2O_3 (11.21%), SiO_2 (0.21%), other impurities (6.35%)

Sulfuric acid (H_2SO_4, 98%), thiourea (CH_4N_2S, 99%), ammonium hydroxide (NH_4OH), glucose ($C_6H_{12}O_6$), sulfur (S), ethanol (C_2H_5OH), were purchased from Factory Co., Ltd (China), tetracycline hydrochloride ($C_{22}H_{24}O_8N_2$.HCl, 96.09%) was obtained from Drug Testing Institute in Ho Chi Minh City (Vietnam).

Synthesis of C, N, S doped TiO_2 materials

Take 2.27 grams of $TiOSO_4$ and a determined amount of thiourea (with the molar ratio of thiourea /TiO_2 = 2:1) were put in a Teflon flask then dissolved with distilled water. Put the Teflon flask in the autoclave, and perform 180 ^oC hydrothermal for 12 hours.

After hydrothermal, the autoclave was allowed to cool naturally to room temperature. Filter the resulting white precipitate and wash it several times with distilled water until the filtrate has a constant pH. The obtained product was dried and calcined at 500 ^oC for 1 hour to get TH-TiO_2 material.

The synthetic single-element doping samples are similar to TH-TiO_2 materials. However, they replace thiourea with NH_4OH, glucose, and sulfur solutions in ethanol too, in turn, introduce nitrogen into the crystal structure of TiO_2 (N- TiO_2), C-doped TiO_2 material (C-TiO_2), sulfur-doped material (S-TiO_2). The mass of the doping agents was calculated based on the number of moles of each doping element in the TH-TiO_2 sample.

Photocatalytic activity

The catalytic activity of C-TiO_2, N-TiO_2, S-TiO_2, and TH-TiO_2 were estimated through the decomposition of tetracycline (30 mg/L) and the catalytic mass (0.6 g/L). The mixture was stirred in the dark for 30 minutes to reach the adsorption/desorption equilibrium, then illuminated with a 60W filament lamp (filter cut-off λ <400 nm). The remaining tetracycline concentration was determined by the HPLC-UV method on Thermo Scientific series 3300 HPLC (Thermo Scientific Technologies, CA, USA) (λ_{max} = 355 nm).

Methods of analysis

The X-ray diffraction (XRD) was conducted in D8 - Advance 5005 with Cu Kα λ = 0.154 nm. The morphology was measured using a scanning electron microscope (SEM) (Nova Nano SEM 450). UV-Vis diffuse reflectance spectroscopy (UV-Vis-DRS) was carried out on Cary 5000 (Varian, Australia). Textural properties of material samples were characterized by nitrogen adsorption/desorption isotherms method using Micromeritics ASAP 2000.

Results and discussion

Characterization of materials

The composition of the material samples C-TiO_2, N–TiO_2, S–TiO_2, and TH-TiO_2 was investigated by an XRD diagram, and the results are presented in Figure 1.

From the figure, the peaks appear at 2θ = 25.3^o; 37.8^o; 48.1^o; 53.9^o; 55.0^o; 62.6^o; 68.8^o; 70.3^o; 75.1^o corresponds to the lattice faces (101), (004), (200), (105), (211), (204), (116), (220), (215) of the TiO_2 anatase phase [13]. Thus,

https://doi.org/10.51316/jca.2022.035

it can be seen that the use of different doping agents does not affect the crystal structure of the material.

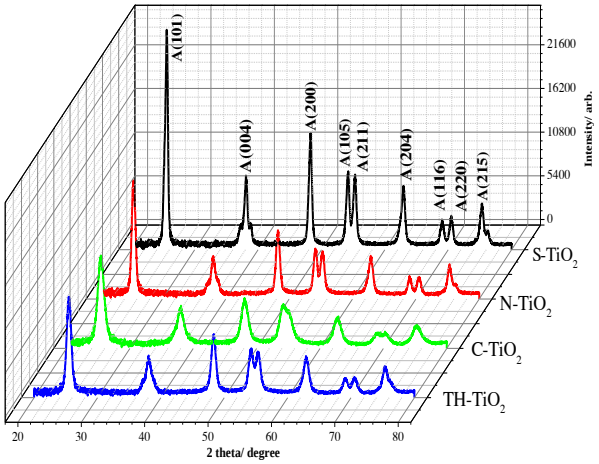

Figure 1: XRD patterns of C, N, S modified TiO_2 samples

The textural properties of the obtained materials were investigated using nitrogen adsorption/ desorption isotherms (Figure 2)

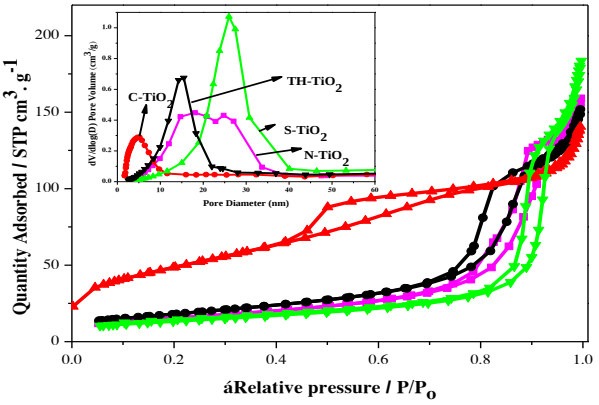

Figure 2: Nitrogen adsorption-desorption isotherms at 77K; the inset presents pore size distribution of S-TiO_2, N-TiO_2, C-TiO_2, TH-TiO_2

The curves of C-TiO_2 material belong to type IV with type H2 loops. According to IUPAC classification, the remaining modified TiO2 materials belong to type V with type H1, all characterized by the mesoporous structure formed by intersecting particles [14], [15]. The doping of C, N, and S elements into the TiO_2 matrix changed the specific surface area, with 47.36, 55.19, 175.64, and 73.47 m^2/g for the respective materials S-TiO_2, N-TiO_2, C-TiO_2, TH-TiO_2 as calculated by the BET model.

The isothermal adsorption-desorption curve begins to condense at a relative pressure P/Po of about 0.7 for the TH-TiO_2, N-TiO_2 samples and about 0.8 for the S-TiO_2 sample, indicating that the material has a small size. Relatively large capillaries (mean diameters of capillaries calculated by the BJH method are 13.81, 16.58, and 24.30 nm, respectively). Meanwhile, the adsorption-desorption curve of C-TiO_2 begins to condense at a relative pressure P/Po of about 0.4, indicating that the material has a small capillary size (the average diameter of the capillaries in the BJH method is 5.31 nm).

The capillary size distribution of TH-TiO_2, C-TiO_2 and N-TiO_2 (Figure 2 inside) shows that the pore size is distributed in a narrow range, indicating that the material has a reasonably uniform pore size. The capillary size distribution of S-TiO_2 extends over 30 nm, corresponding to a relatively large but uneven average capillary.

The characteristic parameters of modified TiO_2 material samples determined by the BET nitrogen adsorption-desorption isotherm method are summarized in Table 1.

Table 1: Characteristic parameters of samples of TiO_2 materials modified by BET model.

Catalysts samples	Specific surface area (S_{BET})(m^2/g)	Pore volume (cm^3/g)	Pore diameter (nm)
TH-TiO_2	73.47	0.248	13.81
C-TiO_2	175.64	0.228	5.31
N-TiO_2	55.19	0.258	16.58
S-TiO_2	47.36	0.273	24.30

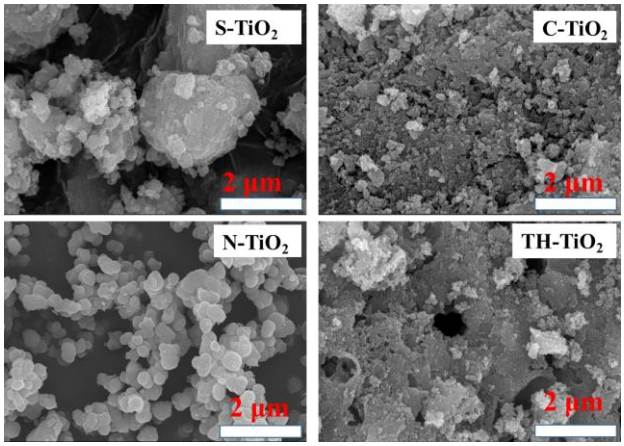

Figure 3: SEM images of S-TiO_2, C-TiO_2, N-TiO_2, TH-TiO_2 samples

Many studies have shown that the activity of the catalyst depends a lot on the surface properties: a

large surface area and a small capillary diameter will create conditions for the reactant molecules to contact more particles. Active centers on the surface, limiting the recombination of photogenerated electrons and holes, increasing the catalytic activity of the material [16], [17], [18].

The surface morphology of the photocatalysts S-TiO_2, C-TiO_2, N-TiO_2, and TH-TiO_2 was studied through SEM images. Figure 3 shows the surface image of high-resolution microparticles with medium-sized spherical particles ranging from 9 to 17 nm.

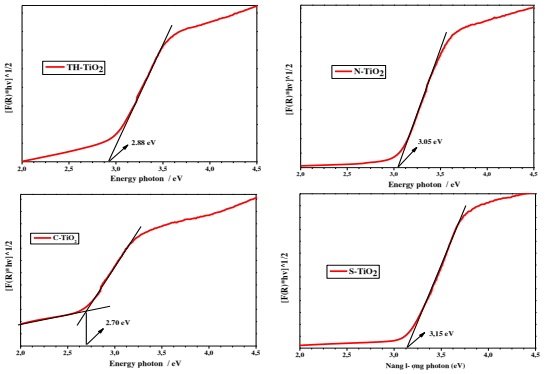

Figure 4: The plot of the Kubelka-Munk function for TH-TiO_2, S-TiO_2, C-TiO_2, N-TiO_2, TH-TiO_2 from UV-Vis-DRS spectra

The bandgap energy is defined explicitly by the Kubelka–Munk function (Figure 4). The bandgap energy of S-TiO_2, N-TiO_2, C-TiO_2, and TH-TiO_2 samples calculated by the Kubelka-Munk function are 3.15, 3.05, 2.7, and 2.88 eV, respectively. The substitution, insertion, and formation of new bonds caused a redshift in the bandgap energies of the doped samples. The ability to absorb light expands to the visible region, and the reduced bandgap energy is necessary to improve the photocatalytic activity of the materials. It can be predicted that the photocatalytic activity will increase gradually from S-TiO_2, N-TiO_2, TH-TiO_2, and C-TiO_2. This prediction is consistent with the prediction made in the BET analysis.

Catalytic activity

From Figure 5a, it is shown that TH-TiO_2 material exhibits the best photocatalytic activity with TC decomposition efficiency above 96%. The two samples, N-TiO_2 and S-TiO_2, performed relatively poorly in the visible light region.

Although the surface area is more extensive and the bandgap energy is smaller than that of S-TiO_2, the photocatalytic activity of N-TiO_2 is worse than that of S-TiO_2, which contradicts the above hypotheses. The test results of the isoelectric point of N-TiO_2 materials have clarified the above contradiction. N-TiO_2 materials are synthesized in an NH_4OH environment with pHpzc = 8. In a primary setting, the following equilibria occur, increasing the negatively charged centers on the material's surface [19], then there is the appearance of N-TiO_2 materials.

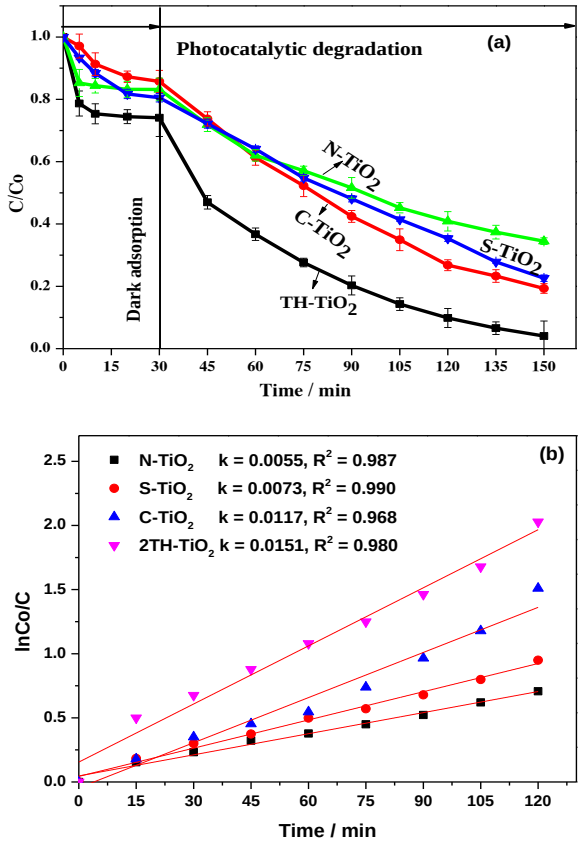

Figure 5: a) Kinetics of TC decomposition reaction; b) Plot of Langmuir-Hinshelwood model on S-TiO_2, N-TiO_2, C-TiO_2 TH-TiO_2.

(Conditions: $m_{catalyst}$ = 0.6 $g.L^{-1}$; concentration of TC = 30 ppm, adsorption time = 30 min)

There is a repulsive interaction between the anionic form of tetracycline and the negatively charged material surface, reducing the adsorption capacity of tetracycline, thereby reducing the tetracycline treatment efficiency.

$$-Ti-O-H+OH^- \rightarrow -Ti-O^- + H_2O$$

$$-Ti-N-H_2+OH^- \rightarrow -Ti-NH^- + H_2O$$

Another great point, C-TiO_2 material has a small crystal size, large specific surface area, and band gap is smaller than TH-TiO_2 material, so it is predicted to have the best photocatalytic activity. However, the

photocatalytic efficiency of tetracycline degradation is lower than that of TH-TiO_2 material. This is due to the high adsorption efficiency of the C-TiO_2 sample and the material's ability to adsorb organic matter well. Causing a light-blocking effect, hindering the light absorption process of the material, making the degradation efficiency of tetracycline decrease [20], [21]. The Langmuir-Hinshelwood model was employed to analyze the kinetics data in which the linear plot of $\ln(C_t/C_0)$ *vs. t* is constructed. Figure 5b presents the Langmuir-Hinshelwood plots at different concentrations. The high determination coefficients, R^2 (0.99 – 1), confirm that the kinetic degradation reaction of TC over S-TiO_2, N-TiO_2, C-TiO_2, and TH-TiO_2 fixed well in the Langmuir-Hinshelwood model.

Conclusion

This study demonstrated the doping of S, N, C, and tridoping S-N-C into TiO2 extracted from ilmenite ore by a hydrothermal process with thiourea. The S-N-C-tridoped TiO_2 exhibited an excellent catalytic activity towards the complete mineralization of tetracycline. The bandgap value of TH-TiO_2 is 2.88 and gave the highest TC decomposition efficiency of 96% after 120 minutes of reaction. This is one of the research directions on materials with potential applications in the water environment treatment process.

References

1. Palominos R. A., Mondaca M. A., Giraldo A., Peñuela G., Pérez-Moya M., and Mansilla H. D., Catalysis Today 144 1-2 (2009) 100-105. https://doi.org/10.1016/j.cattod.2008.12.031
2. Bacsa R., J. Kiwi, T. Ohno, P. Albers, and V. Nadtochenko, (in E), The Journal of Physical Chemistry B 109 12 (2005) 5994-6003. https://doi.org/10.1021/jp044979c
3. Addamo M. et al., in J. Appl. Electrochem 35 (2005) 765–774. https://10.1007/s10800-005-1630-y
4. Khan M.H., Bae H., and Jung J.Y., (in E), J. Hazard Mater 181 1 (2010) 659–665. https://doi.org/10.1016/j.jhazmat.2010.05.063
5. Dobaradaran S. et al., (in E), Iran J Environ Health Sci Eng 7 4 (2010) 307–312.
6. Gotvajn A. Z., Bistan M., Tisler T., Englande A. J., and Zagorc-Koncan J., in Int J Environ Sci Technol 10 (2013) 1141–1148. https://doi.org/10.1007/s13762-012-0153-4
7. Fujishima A., Hashimoto K., and Watanabe T., in A Revolution in cleaning technology (1999) 14-21.
8. N. T. Lan et al., Journal of Nanomaterials 2020, (2020). https://doi.org/10.1155/2020/1523164
9. J. Atanelov, C. Gruber, and P. Mohn, Computational Materials Science 98 (2015) 42-50. https://doi.org/10.1016/j.commatsci.2014.10.041
10. S. Sakthivel and H. Kisch, Angewandte Chemie International Edition 42 40 (2003) 4908-4911. https://doi.org/10.1002/anie.200351577
11. F. Tian and C. Liu, The Journal of Physical Chemistry B 110 36 (2006) 17866-17871. https://doi.org/10.1021/jp0635462
12. J. C. González-Torres, E. Poulain, V. Domínguez-Soria, R. García-Cruz, and O. Olvera-Neria, International Journal of Photoenergy 2018, (2018), https://doi.org/10.1155/2018/7506151
13. L. G. Devi and R. Kavitha, (in E), Materials Chemistry and Physics 143 3 (2014) 1300-1308. https://doi.org/10.1016/j.matchemphys.2013.11.038
14. K. S. W. Sing, (in E), Pure and applied chemistry 57 4 (1985) 603-619. https://doi.org/10.1351/pac198557040603
15. M. D. Donohue and G. L. Aranovich, (in E), Fluid Phase Equilibria 158 (1999) 557-563, https://10.1016/S0378-3812(99)00074-6.
16. H. Zhang et al , RSC Advances 5 129 (2015) 107150-107157. https://doi.org/10.1039/C5RA23743B
17. L. Jingpeng et al., (in E), RSC Advances 7 87 (2017), 55131-55140. https://10.1039/C7RA10103A
18. X. Zhu, Z. Liu, J. Fang, S. Wu, and W. Xu, (in E), Journal of Materials Research 28 10 (2013) 1334-1342. https://doi.org/10.1557/jmr.2013.92
19. Y. Huynh and N. Le, Science and Technology Development Journal 18 (2015) 81-91, https://10.32508/stdj.v18i1.1037.
20. N. Kannadasan, N. Shanmugam, S. Cholan, K. Sathishkumar, G. Viruthagiri, and R. Poonguzhali, Materials characterization 97 (2014) 37-46. https://doi.org/10.1016/j.matchar.2014.08.021
21. N. F. Djaja and R. Saleh, Materials Sciences and Applications 4 02 (2013) 145. https://10.4236/msa.2013.42017